Simultaneous identification of backlash amount and linear characteristics with hybrid identification of time-series data and frequency response data

Ryohei Kitayoshi*a) Student Member, Hiroshi Fujimoto** Senior Member

The purpose of this paper is to propose hybrid identification with time-series data and Frequency Response Data (FRD) for estimation of backlash amount and linear characteristics of the plant. Conventionally, it is difficult to estimate linear characteristics of the plant with backlash because impact due to the gears causes high frequency noise and distorts FRD. Therefore, we propose a method to precisely estimate the linear characteristics of plant by separating the linear characteristics and backlash from the time-series data. To enable precise estimation of linear properties, the proposed method eliminates the effect of nonlinearity from input and output time series data and reconstructs the frequency response data. Normally, another experiment is required to measure the backlash amount, but Bayesian estimation is used to efficiently estimate the backlash from time series data that measure the frequency response characteristics. The effectiveness of the proposed method was confirmed from input/output data acquired from a torsion test machine with backlash.

Keywords: backlash, hybrid identification, time-series data, Frequency Response Data (FRD), torsion test machine

1. Introduction

In recent years, the demand for factory automation has increased with the rise in wages in emerging countries. As a result, the demand for servomotors is also increasing rapidly, and they are being used in large, low-rigidity equipment and equipment with backlash. In particular, backlash is a major cause of lowering the positioning accuracy of machines, and control methods have been proposed to suppress the harmful effects of backlash.

As a control method, Ma et al. proposed a control method that uses a fractional-order PID controller to suppress oscillations due to backlash [1]. Calvini et al. adjusted the controller parameters with heuristics method: PSO (Particle Swarm Optimization) [2]. In addition, Yang et al. used the shaft torque compensator to limit the shaft torque caused by the gear collisions [3]. Yamada et al. used the load-side enconder, identified the backlash width and inprove backdrivability [4]. Moreover, Yamada et al. proposed of FF (FeedForward) controller which was based on a sigmoid function, joint torque FB (FeedBack) controller, and realized compensation of the effect of backlash [5]. Wakui et al. applied the joint torque control to the vibration suppression of a driving shaft of an electric vehicle with backlash and illustrated usefulness for industrial applications [6].

On the other hand, various methods have been proposed to identify the backlash amount. As an identification method, Gebler et al. enabled to measure the backlash amount with only motor current and without output load-side sensor [7]. Villwock et al. measured the backlash amount by integrating the velocity difference between the load-side and drive side velocities from the time the gears began to separate to the time the gears made contact again [8] [9].

However, for suppression of the oscillation due to backlash in the most of the previous researches, it is necessary to know the precise linear characteristics of the plant and the backlash

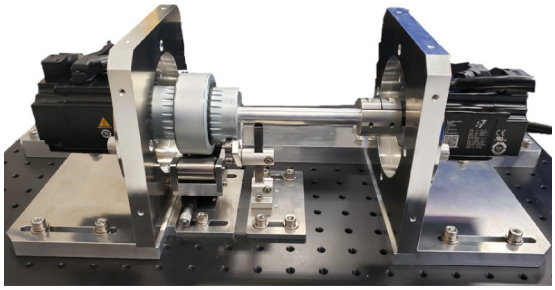

Fig. 1. Overview of the torsion test machine with backlash

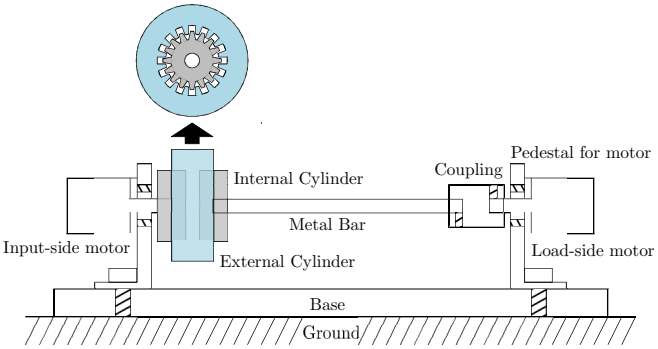

Fig. 2. Schematic drawing of the torsion test machine with backlash

a) Correspondence to: Ryohei.Kitayoshi@yaskawa.co.jp
* Corporate Research & Development Center YASKAWA Electric Corporation, 9-10 Tokodai 5 Chome, Tsukuba, Ibaraki, Japan 300-2635, Japan
** The University of Tokyo, 5-1-5 Kashiwanoha, Kashiwa, Chiba, 277-8561, Japan

amount. Normally, a separate experiment is required to measure the amount of backlash, but our proposed method enables to estimate the linear characteristics by eliminating the effect of backlash from the input/output data to measure the frequency response. The backlash amount is estimated from time series data by Bayesian optimization. The effectiveness of the proposed method is verified by using a torsional test machine with backlash.

In the following, we describe the structure of the paper. In section 2, mechanism and dynamic model of the torsion test machine are described. In section 3, the proposed method to identify the linear characteristics and backlash simultaneously is explained. In section 4, the backlash measurement result and the identification result based on the proposed method are compared. In section 5, a summary of this paper is described.

2. Torsion test machine with backlash

The torsion test machine is an experimental machine produced to validate the proposed identification method. In following, the torsion test machine is called "test machine". The overview of the test machine is shown in Fig.1.

2.1 Mechanical configuration The test machine consists of four parts in Fig.2: two motors, a gear coupling, a metal bar, and a coupling. The two motors are put on both ends of the metal bar which are fastened with the gear coupling and the coupling. The gear coupling consists of two internal cylinders and an external cylinder. Between the internal cylinder and the external cylinder, there is backlash whose amount is 0.51 deg.

The input-side/load-side motors are YASKAWA Electric products (motor model: SGM7A-02A7A and servo drive model: SGD7S-1R6A) with a 24-bit encoder. The input-side motor drives the test machine, and the load -side motor measures the load side angle with the encoder.

2.2 Two-mass system with backlash A dynamic model of the test machine is expressed with two-mass system including backlash. A block diagram of the two-mass model is shown in Fig.3 and parameters and variables are on the Table1. The load-side inertia is driven by the joint torque which is effected by the backlash.

In this paper, the backlash model is expressed in a dead zone whose width is equal to the backlash amount shown in (1) and Fig.4 [10]. Representing a backlash model based on the dead zone has recently become a common practice and and there is an application example to modeling of the elastic robot joint [11]. In addition, there is an attempt to represent the plant including backlashes as the extended Wiener–Hammerstein system [12].

The backlash amout and input to the dead zone are expressed in ϵ and x_s respectively. In the above, the linear dynamic model of the two-mass system is represented in (2)–(5). Transfer functions from torque reference T_{ref} to input-side velocity V_m and load-side velocity V_ℓ are in (6) and (7). Their coefficients are represented with the parameters of the two-mass system from (8) to (14). If the frequency response data are obtained and (6) can be modeled, it is possible to work the parameters backwards.

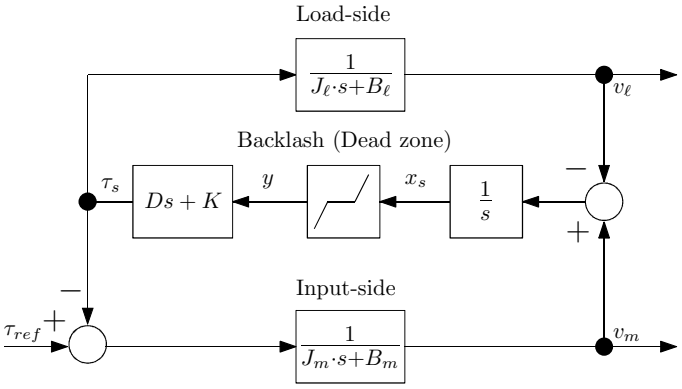

Fig. 3. Two mass system with backlash

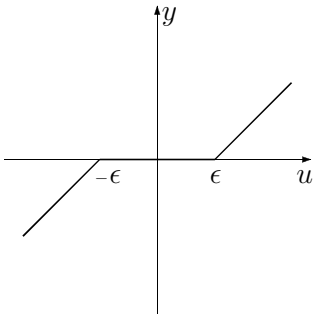

Fig. 4. Backlash model expressed with dead zone

$$y = \begin{cases} x_s - \epsilon & \text{for} \quad x_s > \epsilon \\ 0 & \text{for} \quad -\epsilon \le x_s \le \epsilon \\ x_s + \epsilon & \text{for} \quad x_s < -\epsilon \end{cases} \cdots\cdots (1)$$

$$J_m \cdot \ddot{x}_m = \tau_{ref} - B_m \cdot \dot{x}_m - \tau_s \cdots\cdots (2)$$

$$J_\ell \cdot \ddot{x}_\ell = \tau_s - B_\ell \cdot \dot{x}_\ell \cdots\cdots (3)$$

$$\tau_s = (D \cdot s + K) \cdot y \cdots\cdots (4)$$

$$y = x_m - x_\ell \cdots\cdots (5)$$

$$\frac{V_m}{T_{ref}} = \frac{b_2 \cdot s^2 + b_1 \cdot s + b_0}{s^3 + a_2 \cdot s^2 + a_1 \cdot s + a_0} \cdots\cdots (6)$$

$$\frac{V_\ell}{T_{ref}} = \frac{c_0}{s^3 + a_2 \cdot s^2 + a_1 \cdot s + a_0} \cdots\cdots (7)$$

$$c_0 = \frac{K}{J_\ell \cdot J_m} \cdots\cdots (8)$$

$$b_2 = \frac{1}{J_m} \cdots\cdots (9)$$

$$b_1 = \frac{D + B_\ell}{J_m \cdot J_\ell} \cdots\cdots (10)$$

$$b_0 = \frac{K}{J_m \cdot J_\ell} \cdots\cdots (11)$$

$$a_2 = \frac{(D + B_\ell) \cdot J_m + (D + B_m) \cdot J_\ell}{J_m \cdot J_\ell} \cdots\cdots (12)$$

$$a_1 = \frac{(J_m + J_\ell) \cdot K + (B_m + B_l) \cdot D + B_\ell \cdot B_m}{J_m \cdot J_\ell} \cdots\cdots (13)$$

$$a_0 = \frac{(B_m + B_\ell) \cdot K}{J_m \cdot J_\ell} \cdots\cdots (14)$$

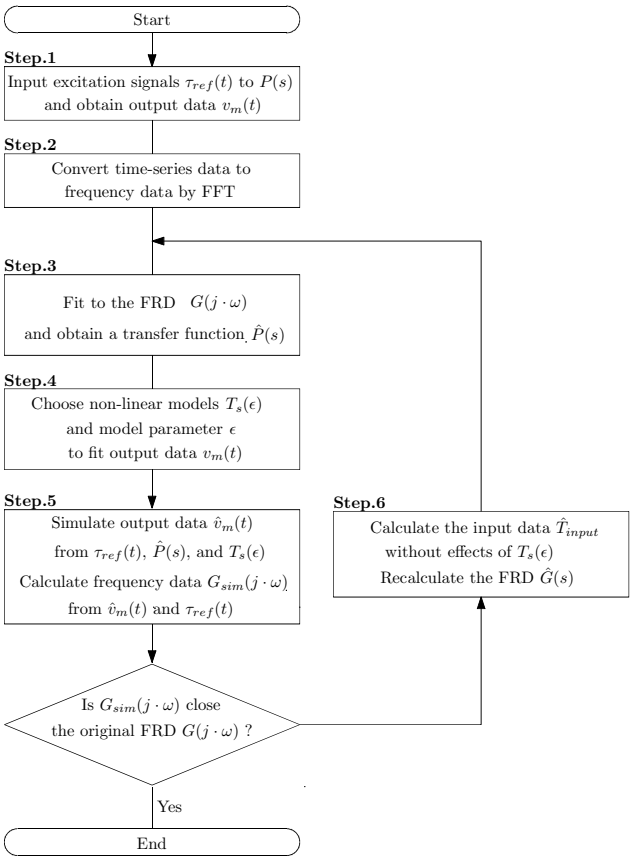

Fig. 5. Flowchart of the proposed hybrid system identification

Table 1. Paramters and variables of two-mass system

Symbol	Item	Units
J_m	Input-side inertia	kg·m^2
J_ℓ	Load-side inertia	kg·m^2
B_m	Input-side viscous coefficient	N·m·s / rad
B_ℓ	Load-side viscous coefficient	N·m·s / rad
K	Elastic coefficient	N·m / rad
D	Damping coefficient	N·m·s / rad
X_m	Input-side angle	rad
X_ℓ	Load-side angle	rad
T_{ref}	Torque reference	N·m
T_s	Joint torque	N·m

The model parameters can be calculated from the coefficients of the transfer function using the following equations.

$$D = -\frac{J_m\cdot(J_m - J_\ell)\cdot b_2 - J_m\cdot a_0}{2\cdot\omega_{a1}^2} \cdots\cdots\cdots\cdots (15)$$

$$B_m = -\frac{J_m\cdot(J_m + J_\ell)\cdot b_2 - J_m\cdot a_0}{2\cdot\omega_{a1}^2} \cdots\cdots\cdots\cdots (16)$$

$$B_\ell = \frac{J_m\cdot(J_m + J_\ell)\cdot b_2 - J_m\cdot a_0}{2\cdot\omega_{a1}^2} \cdots\cdots\cdots\cdots (17)$$

3. Proposed hybrid identification method

In this section, the proposed hybrid system identification with time-series data and frequency response data is explained. The proposed method consists of six steps shown in Fig.5.

3.1 Flow of the proposed identification method

Step.1: Measurement of time-series input/output data

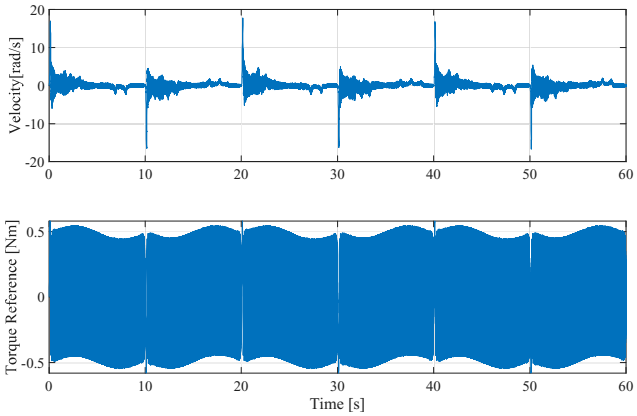

Fig. 6. Measurement of time-series data of torque reference $\tau_{ref}(t)$ and motor velocity $v_m(t)$

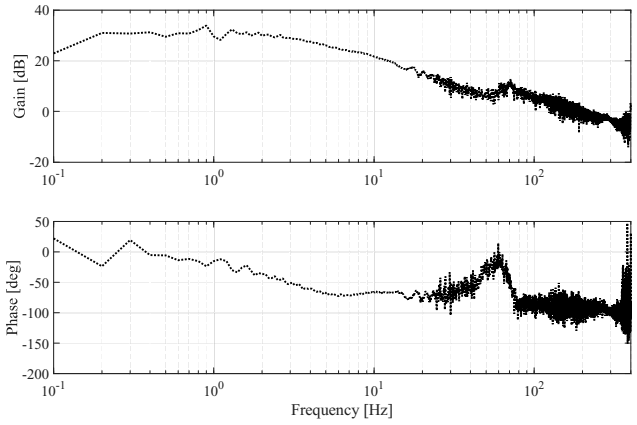

Fig. 7. Frequency Reseponce Data (FRD) of the test machine (input: torque reference $\tau_{ref}(t)$, output: velocity $v_m(t)$)

The excitation torque signal $\tau_{ref}(t)$ is input to the plant, and the output velocity data $v_m(t)$ is acquired. The excitation signal is a chirp signal in (18) and (19). The frequency of the signal $\omega(t)$ changes from 0.1 Hz to 400 Hz, and the measurement time t_{meas} and the sampling period are 10 s, 125 µs, respectively. The initial frequency ω_0 is $0.1\cdot 2\pi$ rad/s, and the final frequency ω_1 is $400\cdot 2\pi$ rad/s. The initial phase of the signal ϕ_0 is 0 deg. The amplitude of the signal A is 0.0764 Nm (12% of the rated motor torque).

$$\tau_{ref}(t) = A\cdot\sin\Big(\omega(t)\cdot t + \phi_0\Big) + 3A\sin(0.1\cdot 2\pi t)\cdot \quad (18)$$

$$\omega(t) = \omega_0 + (\omega_1 - \omega_0)\cdot\frac{t}{t_{meas}} \quad (0\le t\le 10)\ \cdot\cdot \quad (19)$$

Step.2: Obtaining Frequency Response Data (FRD)

Fourier transform is applied to the time-series input/output data $\tau_{ref}(t)$, $v_m(t)$ to acquire the FRD of the plant $G(j\cdot\omega)$. The frequency resolution is 0.1 Hz. The obtained FRD is shown in Fig.7.

Step.3: Estimation of transfer function

The linear transfer function $\hat{P}(s)$ is estimated by fitting for the FRD: $G(j\cdot\omega)$. The fitting method is based on least-squares [13]. The numerator and denominator degree was set as 2 and 3 ($n = 2, m = 3$) because there is at least one vibration mode from the FRD.

$$\hat{P}(s) = \frac{b_n s^n + b_{n-1}s^{n-1} + \cdots b_0}{s^m + a_{m-1}s^{m-1} + \cdots + a_0} \cdots\cdots\cdots\cdots (20)$$

Table 2. Search range of backlash parameter

Symbol	Min	Max	Resolution	Unit
ϵ	0.01	1	0.01	deg

Step.4: Searching of parameters of the nonlinear model based on Bayesian optimization
The nonlinear torsion torque $T_s(\epsilon, t)$ is prepared in (21)–(24) based on the dead zone in Fig.4 and its model parameter ϵ is searched from a search range Λ in Table2 to match the time-series output data $v_m(t)$ and the simulated output data $\hat{v}_m(t)$. The searching method of the nonlinear model and its parameter is Bayesian optimization explained in 3.2.

$$\hat{T}_s = \begin{cases} K \cdot (x_s - \epsilon) & \text{for} \quad x_s > \epsilon \\ 0 & \text{for} \quad -\epsilon \le x_s \le \epsilon \\ K \cdot (x_s + \epsilon) & \text{for} \quad x_s < -\epsilon \end{cases} \cdots\cdots (21)$$

$$\hat{T}_{input} = T_{ref} - \hat{T}_s \cdots\cdots (22)$$
$$\hat{v}_m(t) = \hat{P}(s) \cdot \hat{T}_{input} \cdots\cdots (23)$$
$$\epsilon^* = \arg\min_{\epsilon \in \Lambda} |v_m(t) - \hat{v}_m(t)| \cdots\cdots (24)$$

Step.5: Simulation of the output data based on the estimated transfer function and nonlinear model
To verify the estimation results, output data $\hat{v}_m(t)$ is generated by simulation based on the obtained estimation model $\hat{P}(s)$ in Step.3, the obtained nonlinear model ϵ in Step.4, and the excitation signal $\tau_{ref}(t)$ used in Step.1. Simulated FRD: $G_{sim}(j \cdot \omega)$ is produced from $\tau_{ref}(t)$ and $\hat{v}_m(t)$. If the frequency response data close enough can be reproduced, the identification process is terminated. If it cannot be reproduced, perform Step.6.
Step.6: Calculating input/output data without effect of the nonlinear model and recalculating the frequency data
After removing the nonlinear model's influence from the time-series input/output data, the FRD is regenerated from (25) and (26). The linear transfer function $\hat{P}(s)$ is estimated from the regenerated FRD $\hat{G}(j \cdot \omega)$ again in Step.3.

$$\hat{T}_{input} = T_{ref} - \hat{T}_s \cdots\cdots (25)$$
$$\hat{G}(j \cdot \omega) = \frac{V_m}{\hat{T}_{input}} \cdots\cdots (26)$$

3.2 Bayesian optimization: a search method for parameters of nonlinear model Bayesian optimization is one of the optimization methods for the black-box optimization problem whose objective function is unknown. The representative black-box optimization problem is the hyperparameter search of Neural Networks or Support Vector Machine [14]. Commonly, the random search and the grid search have been used, but Bayesian optimization has been focused as a more efficient search method based on the Gaussian process. In recent years, not only in the field of machine learning but also in the field of control engineering, the application of Bayesian optimization was reported for parameter tuning of the controller in the nonlinear system [15].

Bayesian optimization is expressed in (27)–(30). A vector of hyperparameters is denoted by $\lambda \in \Lambda$. The objective function is denoted by $L(\lambda)$. The expected improvement in (29) and (30) is used as the acquisition function. The improvement of at the combination of the parameters λ is expressed in (28).

$$\lambda^* = \arg\min_{\lambda \in \Lambda} L(\lambda) \cdots\cdots (27)$$
$$I(\lambda) = \max(f_{min} - y, 0) \cdots\cdots (28)$$
$$E[I(\lambda)] = E[\max(f_{min} - y, 0)] \cdots\cdots (29)$$
$$E[I(\lambda)] = (f_{min} - \mu(\lambda))\Phi\left(\frac{f_{min} - \mu(\lambda)}{\sigma}\right) + \sigma\phi\left(\frac{f_{min} - \mu(\lambda)}{\sigma}\right) \cdots\cdots (30)$$

In the above, ϕ and Φ are the standard normal density and distribution function. The symbol μ, σ and f_{min} express the current best value respectively.

$$L(\lambda) = \max(|v_m(t) - \hat{v}_m(t)|) \cdots\cdots (31)$$

4. Experiment for validiation of Hybrid identification

In this section, we compare the results of analyzing the linear characteristics and backlash amount based on the proposed method with measurement result of backlash amount.

4.1 Measurement condition The input-side motor is driven at a constant frequency velocity reference. The frequency of the velocity reference is 0.5 Hz. The amplitude of the velocity reference is 1.5 rad/s.

4.2 Measurement results of Backlash We measured the backlash amout by integrating the velocity difference between the input-side velocity and the load-side velocity [8]. The backlash amout is calculated from (32). A symbol t_1 is the time when the gears separates and t_2 is the time when the gears recontact.

The velocity response is shown in Fig. 11 and 12. When the input-side motor velocity reverses, there is a large difference between the input-side and load-side velocity. In Fig.11, $t_1 = 3.20$ and $t_2 = 3.30$ are set. From Fig.13, backlash amount is $2\epsilon = 0.877$ deg, that is, $\epsilon = 0.439$ deg.

$$2\epsilon = \left| \int_{t1}^{t2} v_m(t) - v_\ell(t) dt \right| \cdots\cdots (32)$$

4.3 Measurement results of input-side inertia and load-side inertia We measured the input-side intertia and the load-side inertia for validation of the proposed method. The input-side and load-side driving shaft were driven freely, and the frequency response data were measured. The frequency response data of input-side and of load-side are shown in Fig.8 and Fig.9. From the frequency response data, the transfer function models were estimated. An estimated model of the input-side is illustrated in (33) and an estimated model of the input-side is illustrated in (34). The input-side inertia is 4.11×10^{-4} kg·m^2 and the load-side inertia is 1.47×10^{-4} kg·m^2.

$$G_{input} = \frac{2432.6}{s + 1.192} \cdots\cdots (33)$$
$$G_{load} = \frac{6795.6}{s + 2.109} \cdots\cdots (34)$$

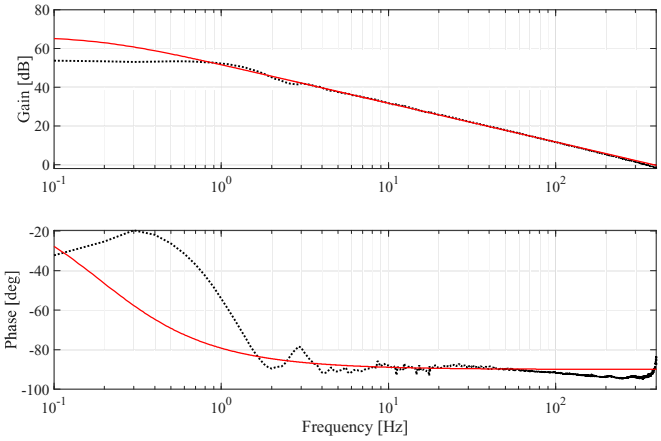

Fig. 8. Frequency response data of only the input-side driving shaft

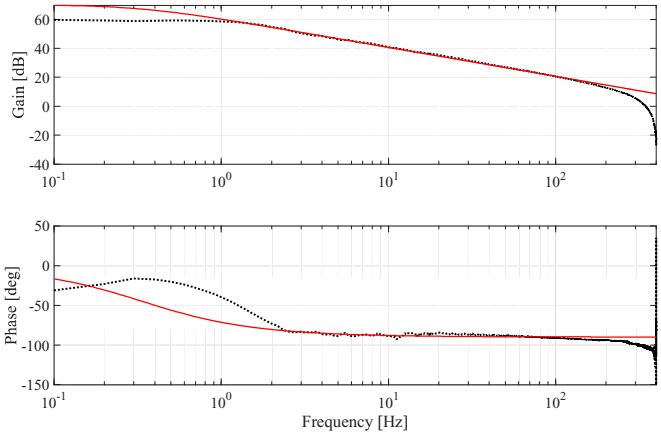

Fig. 9. Frequency response data of only the load-side driving shaft

Table 3. Analysis results of two-mass system

Symbol	Value	Units
J_m	4.78×10^{-4}	kg·m^2
J_ℓ	1.92×10^{-4}	kg·m^2
B_m	0.84×10^{-2}	N·m·s / rad
B_ℓ	0.53×10^{-2}	N·m·s / rad
K	23.10	N·m / rad
D	1.54×10^{-2}	N·m / rad

4.4 Comparison for analysis result and measurement

A comparison between the measurements and the analytical results shows that the input and load side inertia can be estimated with good accuracy. In addition, estimated backlash amount is 0.40 deg in Table.4 while the measurement of the backlash amount is 0.439 deg in 4.2. The estimated backlash amount is close to measurement.

Based on the estimated backlash amount and estimated two-mass system parameters of the two-mass model, input-side velocity was estimated and compared with the measurement of input-side velocity in Fig.14. The estimated transfer function $\hat{P}(s)$ is in (35). The regenerated FRD is shown in Fig.15. In the low-frequency and high-frequency bands, the estimated and measured FRD are fitted, but the gain of the resonant frequency is larger than measurement in the vibration modes. This is because the damping the between gears was low estimated.

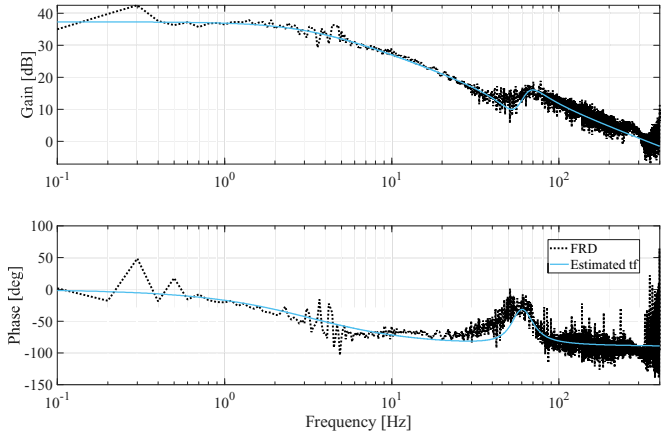

Fig. 10. Comparison for frequency response data (black: experiment data, red dashed: simulation data based on the transfer function fitted to FRD)

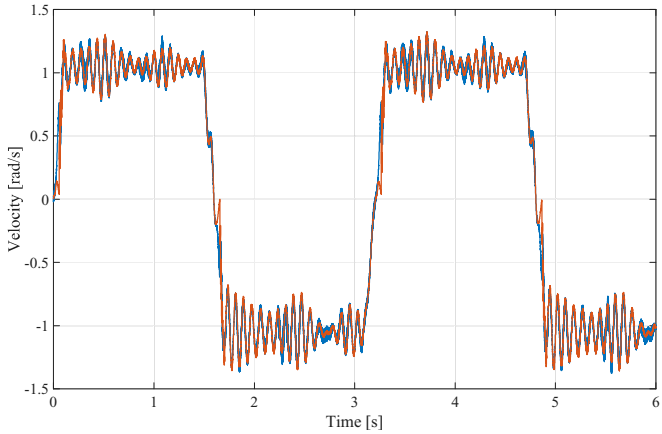

Fig. 11. Time-series data of velocity response (blue line: input-side velocity and red line: load-side velocity)

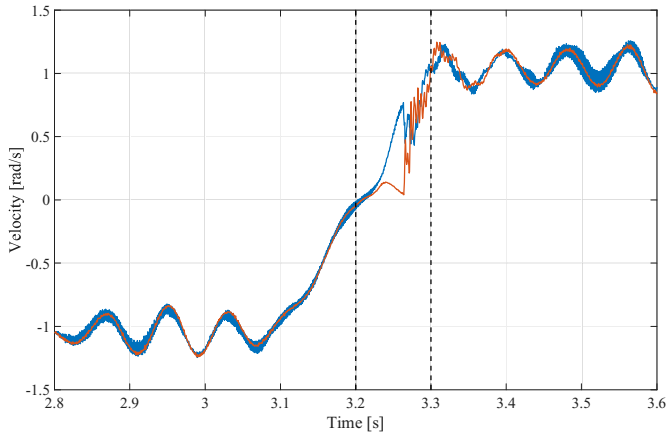

Fig. 12. Time-series data of velocity response from 2.8 s to 3.6 s (blue line: input-side velocity and red line: load-side velocity)

$$\hat{P}(s) = \frac{K}{s(s+20.11)} \cdot \frac{s^2 + 2\zeta_{a1}\omega_{a1}s + \omega_{a1}^2}{s^2 + 2\zeta_{r1}\omega_{r1}s + \omega_{r1}^2} \cdots\cdots \quad (35)$$

5. Conclusion

This paper proposed the hybrid identification method with

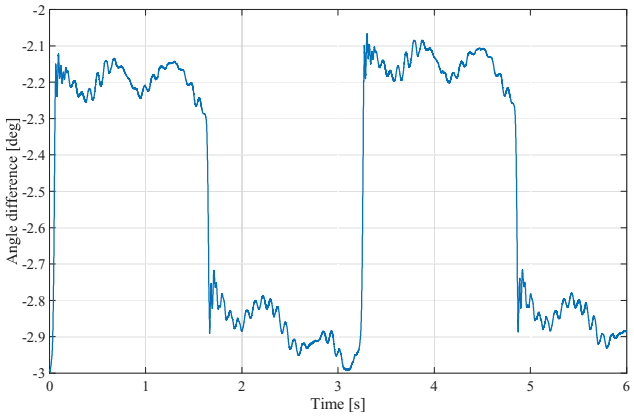

Fig. 13. Measurement data of torsion angle: $x_m - x_\ell$

Table 4. Search results of backlash parameters

Symbol	Value	Unit
ϵ	0.40	deg

Table 5. Analysis results of frequency characteristics

Symbol	Value	Unit
ω_{r1}	$65.8 \times 2\pi$	rad/s
ζ_{r1}	1.67×10^{-1}	-
ω_{a1}	$55.2 \times 2\pi$	rad/s
ζ_{a1}	1.55×10^{-1}	-
K	2.09×10^{3}	-

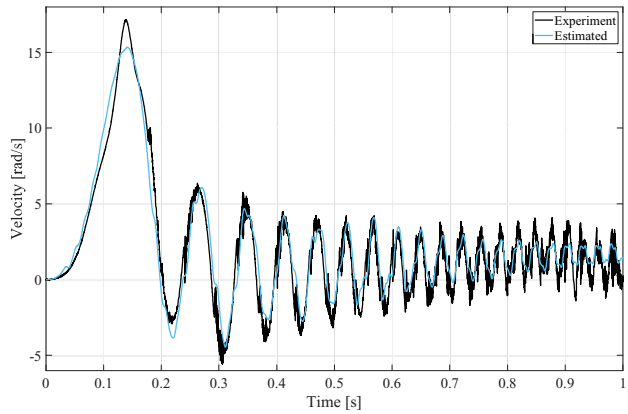

Fig. 14. Comparison for time-series data of velocity between measurement and estimated data

time-series data and frequency response data for obtaining the precise frequency characteristics of the plant and backlash. For validation of the proposed method, we conducted the measurement of backlash amount and frequency response data of the torsion test machine, and the proposed method's analysis results were compared with measurement.

Moreover, Bayesian optimization was used for the efficient searching method of the backlash amount, and we obtained the appropriate value which matched the measurement.

We have planned to automatically adjust the position controller with obtained frequency characteristics and backlash amount. The frequency characteristics are used for the adjustment of the FB controller and the design of the FF controller.

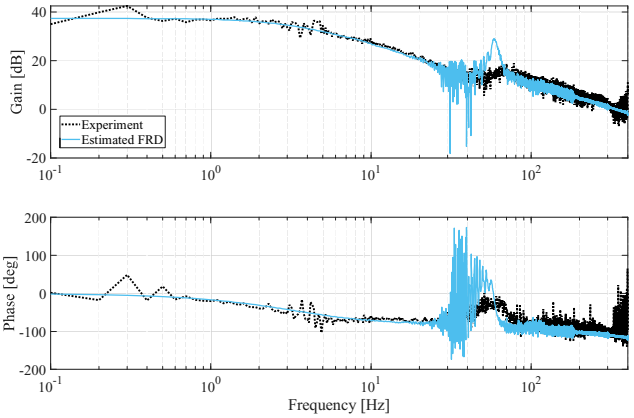

Fig. 15. Comparison for frequency response data between measurement and estimated data

References

(1) C. Ma and Y. Hori, "Backlash Vibration Suppression Control of Torsional System by Novel Fractional Order PIDk Controller," *IEEJ Transactions on Industry Applications*, vol. 124, no. 3, pp. 312–317, 2004.

(2) M. Calvini, M. Carpita, A. Formentini, and M. Marchesoni, "PSO-Based Self-Commissioning of Electrical Motor Drives," *IEEE Transactions on Industrial Electronics*, vol. 62, no. 2, pp. 768–776, feb 2015.

(3) M. Yang, C. Wang, D. Xu, W. Zheng, and X. Lang, "Shaft Torque Limiting Control Using Shaft Torque Compensator for Two-Inertia Elastic System With Backlash," *IEEE/ASME Transactions on Mechatronics*, vol. 21, no. 6, pp. 2902–2911, dec 2016.

(4) S. Yamada and H. Fujimoto, "Proposal of high backdrivable control using load-side encoder and backlash," in *IECON 2016 - 42nd Annual Conference of the IEEE Industrial Electronics Society*. IEEE, oct 2016, pp. 6429–6434.

(5) ——, "Precise joint torque control method for two-inertia system with backlash using load-side encoder," *IEEJ Journal of Industry Applications*, vol. 8, no. 1, pp. 75–83, 2019.

(6) S. Wakui, T. Emmei, H. Fujimoto, and Y. Hori, "Gear Collision Reduction of Geared In-Wheel-Motor by Effective Use of Load-Side Encoder," in *IECON 2019 - 45th Annual Conference of the IEEE Industrial Electronics Society*, vol. 2019-Octob. IEEE, oct 2019, pp. 3615–3620.

(7) D. Gebler and J. Holtz, "Identification and compensation of gear backlash without output position sensor in high-precision servo systems," in *IECON '98. Proceedings of the 24th Annual Conference of the IEEE Industrial Electronics Society (Cat. No.98CH36200)*, vol. 2. IEEE, 1998, pp. 662–666.

(8) S. Villwock and M. Pacas, "Deterministic method for the identification of backlash in the time domain," *IEEE International Symposium on Industrial Electronics*, vol. 4, pp. 3056–3061, 2006.

(9) ——, "Time-Domain Identification Method for Detecting Mechanical Backlash in Electrical Drives," *IEEE Transactions on Industrial Electronics*, vol. 56, no. 2, pp. 568–573, feb 2009.

(10) M. Nordin and P.-O. Gutman, "Controlling mechanical systems with backlash a survey," *Automatica*, vol. 38, no. 10, pp. 1633–1649, oct 2002.

(11) M. Ruderman, S. Member, F. Hoffmann, S. Member, and T. Bertram, "Modeling and Identification of Elastic Robot Joints With Hysteresis and Backlash," vol. 56, no. 10, pp. 3840–3847, 2009.

(12) L. Li and X. Ren, "Parameter identification based on prescribed estimation error performance for extended Wiener – Hammerstein systems," *IET Control Theory & Applications*, vol. 14, no. 2, pp. 304–312, 2019.

(13) Z. Drmač, S. Gugercin, and C. Beattie, "Quadrature-Based Vector Fitting for Discretized H2 Approximation," *SIAM Journal on Scientific Computing*, vol. 37, no. 2, pp. A625–A652, jan 2015.

(14) K. Grąbczewski, *Automated Machine Learning*, ser. The Springer Series on Challenges in Machine Learning, F. Hutter, L. Kotthoff, and J. Vanschoren, Eds. Cham: Springer International Publishing, 2019, vol. 498.

(15) M. Neumann-Brosig, A. Marco, D. Schwarzmann, and S. Trimpe, "Data-Efficient Autotuning With Bayesian Optimization: An Industrial Control Study," *IEEE Transactions on Control Systems Technology*, vol. 28, no. 3, pp. 730–740, may 2020.